Geophysical Prospecting 31, 225–236, 1983.

HIGH-RESOLUTION PREDICTION OF ACOUSTIC IMPEDANCES BELOW BOTTOM-OF-HOLE*

B.B. TAL-VIRSKY and A.A. TABAKOV**

ABSTRACT

TAL-VIRSKY, B.B. and TABAKOV, A.A. 1983, High-Resolution Prediction of Acoustic Impedances below Bottom-of-Hole, Geophysical Prospecting 31, 225–236.

Prediction of acoustic impedances below bottom-of-hole developed in the paper is based on VSP data processing. The pulse form and reflections are deduced from records on the vertical array by the method of subtraction. A deterministic prediction error and a wave-shaping Wiener filter are used to transform the pulse train and reflections into a short symmetrical pulse. Additional broadening of the pulse spectrum is achieved by stacking of seismograms from shots with various dominant frequencies after zero-phase transformation of downgoing waves.

The inversion of seismograms is made after ideal spiking by means of a subtraction procedure. Acoustic impedances deduced are closely related to lithology of rocks below bottom-of-hole.

INTRODUCTION

There are a number of geologic situations which necessitate high-resolution prediction of the geologic section below bottom-of-hole—for example, to recognise the top of overpressured oil- and gas-saturated beds and salt beds. It is often necessary to evaluate the undrilled prospective complexes.

The capabilities of seismic prospecting in solving these problems are based on close relationships between subsurface acoustic parameters and lithology. Many researchers have attempted to estimate these parameters from the seismic responses of the earth, and as a result of these efforts at the close of the seventies a number of procedures were disclosed, which estimate the changes of subsurface acoustic properties as a function of reflection record time (Gogonenkov, Zakharov and Elmanovich 1980, Lindseth 1976, Rainon 1978). The methods still have a number of shortcomings:

* Received August 1981, revision received February 1982.

** State University, Faculty of Geology, Geophysics Department, 700 095 Tashkent, Vuzgorodok, USSR.

0016–8025/83/0400–0225 $02.00

—suppression of multiples is required;
—the incident waveshape is unknown which makes it necessary to make correspondent assumptions for inverse filtering;
—the frequency range of the record is limited by the spectrum of the source wavelet which reduces resolution of the results;
—it is imperative to have a priori subsurface data available in the form of either true velocities for at least one well or the power spectrum of an impulse seismogram.

To solve the formulated problem, the authors use seismic records along vertical profiles in boreholes. Signals with different dominant frequencies from several shots are stacked in order to broaden the pulse spectrum.

In effect, two detectors are sufficient to implement the procedures to be discussed later. However, for practical applications we use the records from 11 detectors with vertical spacing of 15 m. The whole array may be composed of nine positions of three-point arrays, which is moved 15 m up for the next shot providing additional stacking. The shot point should be positioned as near to the well as possible. Observations may be obtained during short-time removal of drilling equipment. The major advantages of this technique are low noise level and recording of the incident and reflected waves through the same channel. It permits one to derive true values of reflection coefficients, as well as to apply different determinant signal transformations, providing a means for effective deconvolution, in particular. Also, the reduction of source pulses with different frequency impulses to zero phase and data stacking allows effective deconvolution to be carried out.

The technique under consideration does not require pre-attenuation of multiples because they are taken into account when the inverse dynamic problem is solved. A number of procedures result in a seismogram approaching the ideal one; it is easily inverted into the time section of acoustic impedances. Figure 1 shows the example of the initial records obtained. The first-arrival line is drawn vertical and binary-gain overlapping is used for display purposes. The incident multiples on this seismogram have vertical coherent line-ups, as opposed to the reflected waves with dipping line-ups.

Separation of the incident and reflected wavefields represents the first processing procedure. The incident waves are subsequently used for the estimation of the source impulse, whereas the reflected waves are used later for prediction of the section by the subtraction method (Nahamkin 1967). To discriminate wavefields, more specific information on time shifts and wave amplitudes is iteratively obtained for each record trace. The source impulse shape is specified iteratively for a whole set of traces.

The jth trace of the seismogram can be represented as a sum of the incident and reflected waves:

$$S_{j,n} = A_j^{\mathrm{d}} \cdot S^{\mathrm{d}}_{n-\phi j^{\mathrm{d}}} + A_j^{\mathrm{u}} \cdot S^{\mathrm{u}}_{n-\phi j^{\mathrm{u}}}, \tag{1}$$

where n is the current index, S^{d} is the incident wave, S^{u} is the reflected wave, A_j^{d} and A_j^{u} are the amplitude coefficients of the incident and reflected waves, respectively, and ϕ_j^{d} and ϕ_j^{u} are the time shifts on the records of the incident and reflected waves

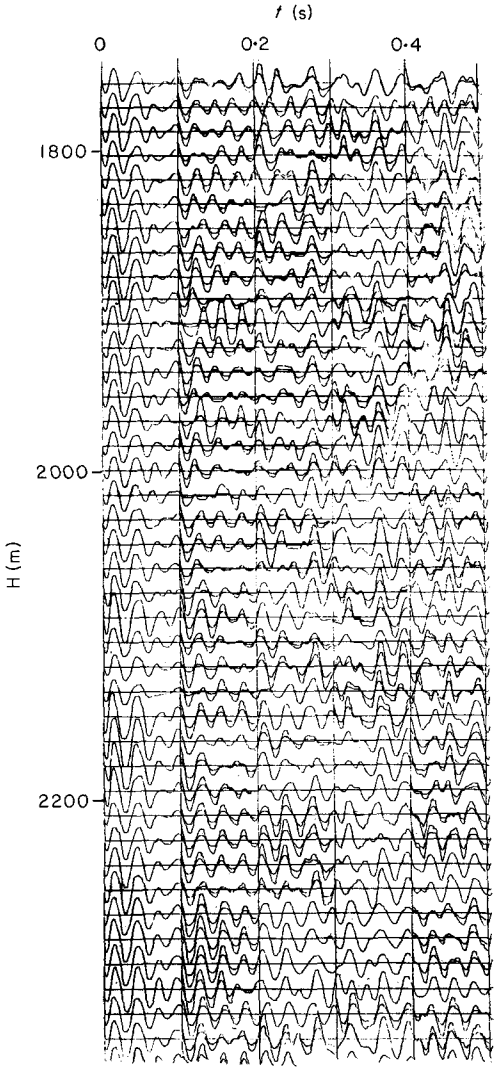

Fig. 1. Initial traces recorded on a vertical profile.

in relation to the corresponding waves on the reference (usually bottom) trace. To separate the incident and reflected waves, it is necessary to find the signal shape, time shifts, and amplitude coefficients for each trace.

To determine the incident wave time shifts ϕ_j^{d}, a zero-order approximation is found from cross-correlation between each of the traces and the reference trace. The traces are then summed using this time shift:

$$\bar{B}_n^{\mathrm{d}} = \sum_{j=1}^{M} S_{j,\, n-\phi_j^{\mathrm{d}}}, \tag{2}$$

where M is the number of traces and $\bar{B}_n^{\mathrm{d}}$ is the incident waveshape estimate. The reflected waves present in the stacked trace are attenuated which permits them to be used for specifying time shifts of the incident wave. To that end, cross-correlation function $\Phi_{j,\tau}$ with each trace is calculated:

$$\Phi_{j,\tau} = \sum_{n=1}^{N} \bar{B}_n^{\mathrm{d}} \cdot S_{j,n-\tau}, \tag{3}$$

where N is the number of samples per trace and τ is the variable time shift. The specified value of ϕ_j^{d} equals to the shift corresponding to the maximum of cross-correlation function. The incident waveshape is specified from (2) using the specified data on time shifts.

The amplitude coefficient of incident waves on each trace is assumed to be equal to the ratio of $\Phi_j^{\max}$ to the energy of incident waves:

$$A_j^{\mathrm{d}} = \Phi_j^{\max} \Big| \sum_{n=1}^{N} (\bar{B}_n^{\mathrm{d}})^2. \tag{4}$$

Similar parameters are determined for the reflected waves using the records where incident waves have been subtracted as the reference traces:

$$S_{j,n}^{\mathrm{u}} = S_{j,n} - A_j^{\mathrm{d}} \cdot \bar{B}_{n+\phi j^{\mathrm{d}}}^{\mathrm{d}}, \tag{5}$$

where $S_{j,n}^{\mathrm{u}}$ is the initial trace after subtraction of the incident waves. As a result, we obtain the parameters $\bar{B}_n^{\mathrm{d}}$, ϕ_j^{u}, and A_j^{u}.

Once the shape and parameters of reflected waves have been determined, these parameters are subtracted from the initial traces and the parameters of incident waves are specified again. The iterations are repeated until the changes in waveshape and parameters become insignificant. The attenuation level for the subtracted wave usually reaches -36 dB after three iterations. Figure 2 depicts the realizations of incident and reflected waves after their discrimination.

The second processing procedure is the predictive deconvolution of the input traces producing signal shortening due to attenuation of ghosts. The determinant predictive filter f^{p} is computed from the signal shape of incident waves $\bar{B}_n^{\mathrm{d}}$:

$$\Phi_{B,B} * f^{\mathrm{p}} = \Phi_{B,B\theta}, \tag{6}$$

where $\Phi_{B,B}$ is the autocorrelation function of incident wave, and $\Phi_{B,B\theta}$ is the autocorrelation function shifted by the amount of lag θ. θ is determined from the condition that the most intensive early portion of the incident wave signal is passed.

The prediction error filter is constructed for conventional Wiener filtering (Robinson and Treitel 1967). Application of the filter to the input traces results in sharp attenuation of the interference of incident and reflected waves outside the passband (fig. 3). The subtraction procedure is again applied to the traces processed with this filter, with the result that the specified incident and reflected waves are obtained as an output.

In the third procedure, the "wave-shaping filter" (Robinson and Treitel 1967) is

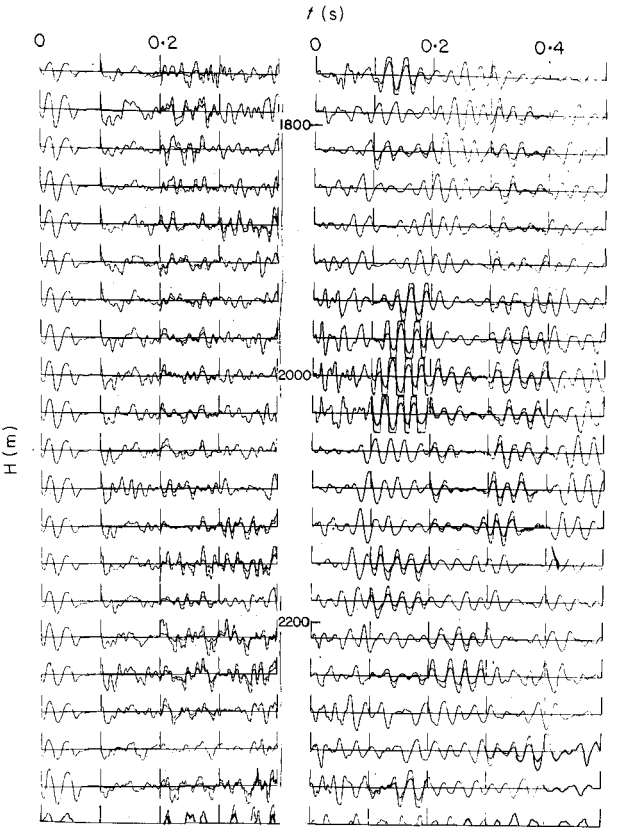

Fig. 2. Separated wave fields. (a) Incident waves, (b) reflected waves.

computed for the incident wave defined in this manner. The desired output is chosen as the autocorrelation of an incident wave multiplied by an exponential function:

$$D_n = \Phi_{|n-\delta|} \cdot \exp\left[-\beta\, \Delta t^2 (n-\delta)^2\right], \tag{7}$$

where D_n is the desired output, $\Phi_{|n-\delta|}$ is the symmetric autocorrelation of the incident wave delayed by the lag δ, β is the exponential parameter, and Δt is the sample interval.

The choice of the desired output in this form is justified by the following considerations. The nature of the filter can be changed from spiking to autocorrelation filter by changing the value of β. In intermediate situations the symmetrical (zero-phase) signal is produced, that is, the spectrum closest to that of the source signal for a given length. It ensures that the filter has low sensitivity to noise.

The additional noise immunity is adjusted by the level of noise autocorrelation added to incident wave autocorrelation. When noise properties are unknown, the

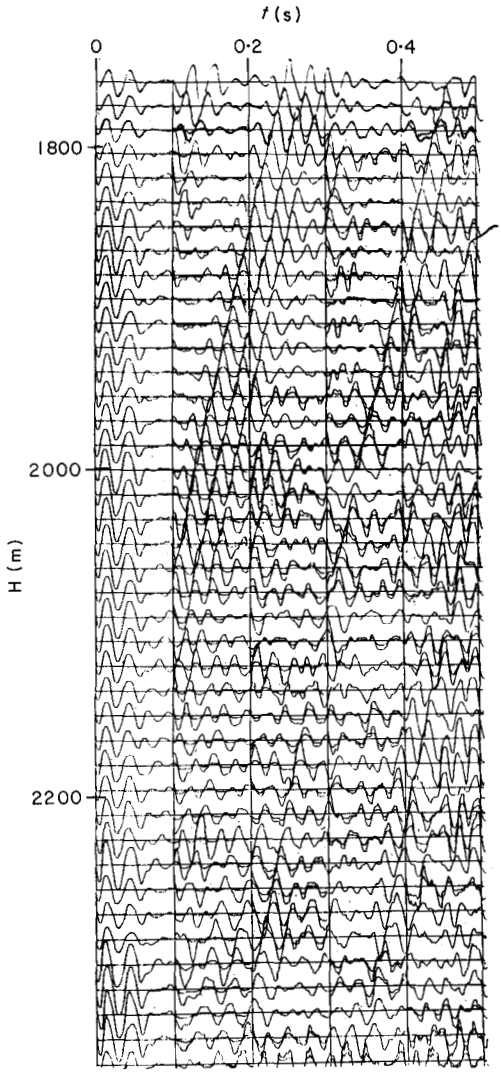

Fig. 3. Initial traces with predictive deconvolution.

first sample of incident wave autocorrelation is corrected. The shaping filter f^{F} is finally computed from the equation

$$(\Phi_{B,B} + \Phi_{N,N}) * f^{\mathrm{F}} = \Phi_{B,D}, \tag{8}$$

where $\Phi_{N,N}$ is the noise autocorrelation, and $\Phi_{B,D}$ is the cross-correlation of the incident wave and the desired output. The experimentally selected lag value δ is approximately equal to 1.5 times the passband range, while the filter length is 2δ. Figure 4 illustrates the noise immunity of the filtering technique and high resolution of the record.

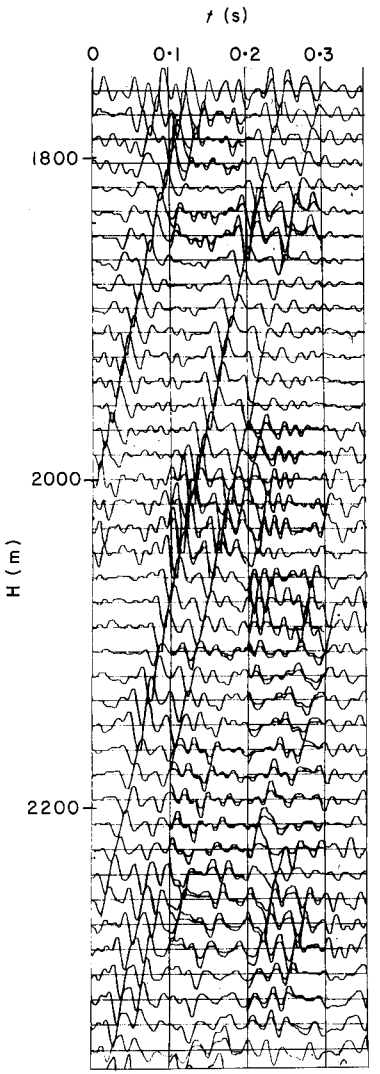

Fig. 4. Reflected waves after predictive deconvolution and wave-shaping filtering.

When source wavelets of different frequency are available, we stack the seismograms processed with the shaping filter. Before summing, the traces are multiplied by the factor permitting equalization of the incident wave energy. When we stack traces containing different frequencies, the spectrum of the incident and reflected waves broadens.

The fourth procedure consists in obtaining the impulse seismogram. The deconvolved reflection trace $\hat{B}_n^{\mathrm{u}}$ is considered as an additive sum of convolutions of the impulse seismogram with the deconvolved incident wave $\hat{B}_n^{\mathrm{u}}$ and noise:

$$\hat{B}_n^{\mathrm{u}} = \hat{B}_n^{\mathrm{d}} * U_n + NS_n, \tag{9}$$

where U_n is the impulse seismogram and NS_n is the residual noise. The above-mentioned subtraction-specification procedure is used to obtain the impulse seismogram. Let us correlate both sides of equation (9) with $\hat{B}_n^{\mathrm{d}}$:

$$\Phi_{B_n^{\mathrm{u}}, \hat{B}_n^{\mathrm{d}}} = \Phi_{B_n^{\mathrm{d}}, \hat{B}_n^{\mathrm{d}}} * U_n + \Phi_{B_n^{\mathrm{d}}, NS_n}. \tag{10}$$

Let us also compute $\Phi_{B_n^{\mathrm{d}}, \hat{B}_n^{\mathrm{d}}}$ and normalize (10) using the maximum value of the

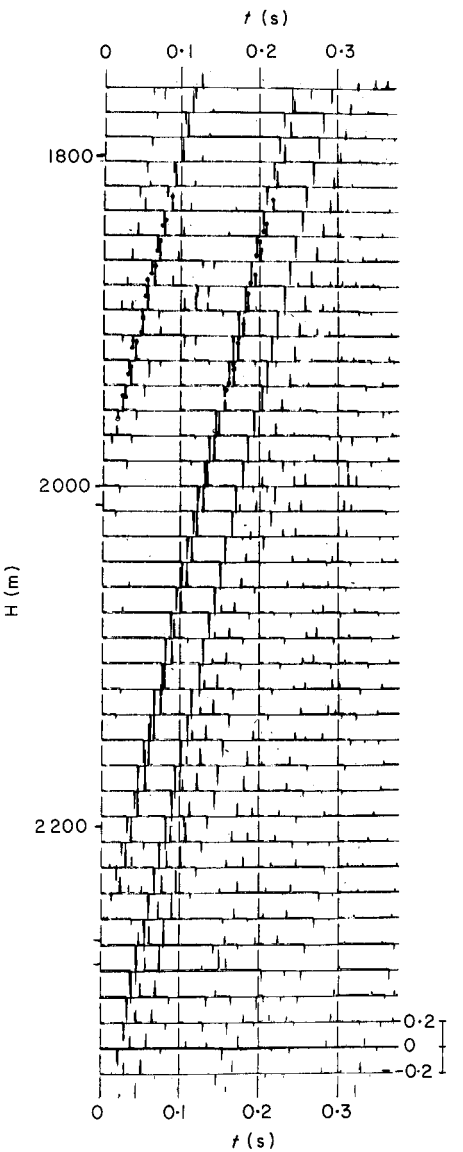

Fig. 5. Impulse seismograms on observation levels.

obtained autocorrelation function. Now the amplitudes of the normalized correlation trace containing reflected waves (10) correspond to reflection coefficients at the observational level. They may be called *apparent reflection coefficients.* The impulse seismogram may be obtained by sequentially estimating and subtracting the contribution of maximum residual apparent reflection coefficients to the correlation seismogram. A unit sample is introduced into the estimated impulse seismogram at the determined maximum time with the relevant intensity.

When the given arrival is subtracted, the residual normalized correlation trace is expressed as

$$\Phi^{R}_{B_n{}^d,\, B_n{}^u} = \Phi_{B_n{}^d,\, B_n{}^u} - \Phi_{B_n{}^d,\, B_n{}^d} * \bar{U}_n, \tag{11}$$

where $\bar{U}_n$ is the estimated impulse seismogram sequentially updated by the maximum reflection coefficients taken into account. When each of the new values of $\bar{U}_n$ is obtained, all its values obtained earlier are iteratively specified. The procedure continues until the maximum sample on the residual trace becomes lower than a prescribed level. Experience has shown that it is desirable to include reflection coefficients higher than 0.0025. Figure 5 shows the impulse seismogram where we detected a 12-m-thick anhydrite bed of 6 km/s and the top of a gas-bearing bed associated with the reef body.

Transformation of the impulse seismogram into the acoustic impedance log is a straightforward two-stage procedure (Alekseyev 1967). The first stage consists of transforming the apparent reflection coefficients ($\bar{U}$) into the true ones (K) with multiples included. The inversed algorithm of Baranov and Kunetz (1960) is used for computation. The true reflection coefficient is defined as the ratio of amplitudes of reflected (R) and incident (J) waves just above the reflector. These amplitudes are determined from the impulse seismogram at the observation level by use of sequential downward recalculation where we take into account reflection and transmission at previously determined reflectors. Figure 6 depicts the calculation scheme used.

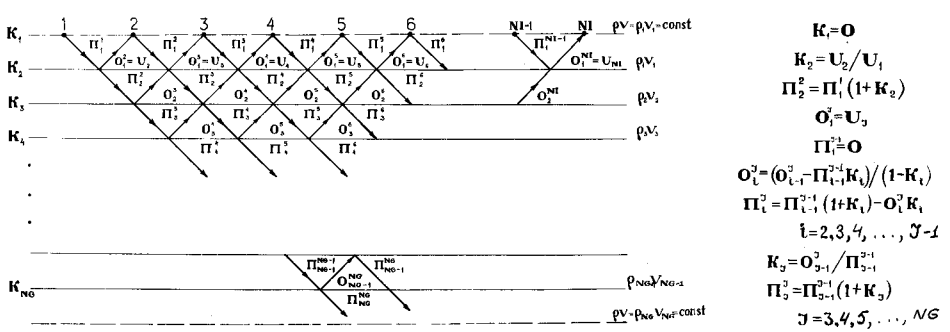

Fig. 6. Determination of true reflection coefficient values from impulse seismogram on observation level. K = reflection coefficients, V_i = P-wave velocities, ρ = densities, U_i = impulse seismograms, Π_i^J and 0_i^J = magnitudes of incident and reflected wave motion within the bed, J = index of estimated reflection coefficient, i = variable index of bed in which the wave motion is computed.

The second stage consists of acoustic impedance calculation from the true impulse seismogram. The acoustic impedance at the observation level is determined from well log data. We use the normal-incidence ray formula:

$$\rho_n V_n = \frac{1 - k_n}{1 + k_n} \rho_{n-1} V_{n-1}. \tag{12}$$

Figure 7 shows the processing results, while fig. 8 demonstrates an example of geologic interpretation.

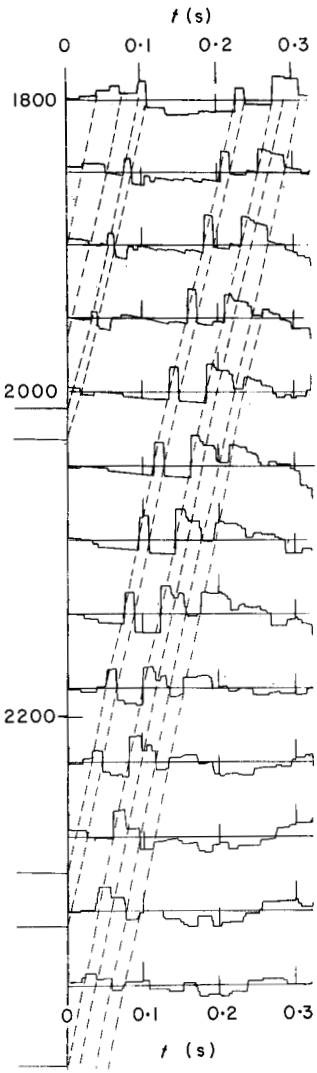

Fig. 7. Acoustic impedances computed for different observation levels (regional component is subtracted).

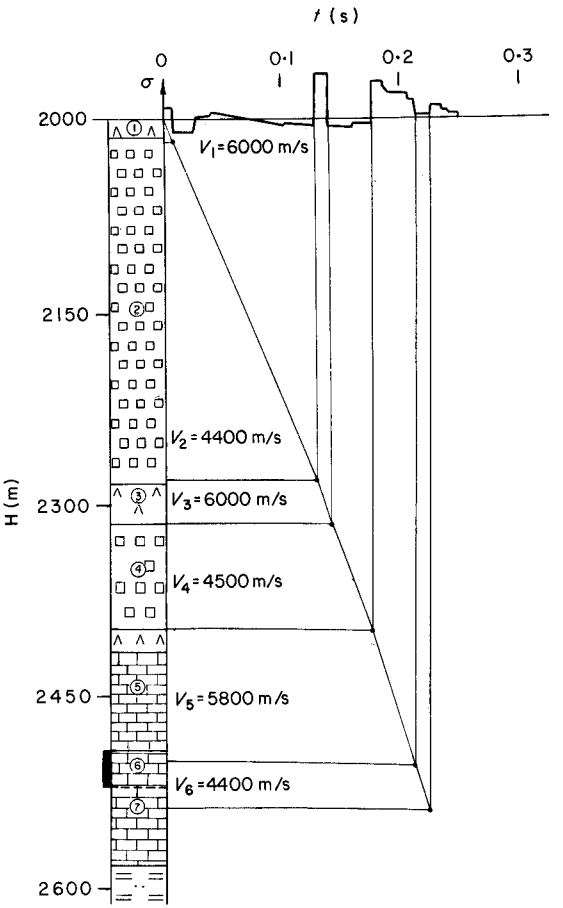

Fig. 8. Example of geologic interpretation of acoustic impedance data.

The stability of the method was tested in a model experiment. The model reflection trace for different source impulses was obtained from the given acoustic impedance log. The solutions were obtained for different noise levels. Similarity to the original log was taken as a measure of efficient solution. The similarity coefficient was found to reach 0.995 for a noise level lower than 5%. The solution is unstable when noise level exceeds 10%.

Statistical methods are used to get higher noise immunity. A number of solutions are computed with modified parameters of deconvolution. The adequate selections are closely correlated, and incorrect ones are randomly distorted. This permits the classification procedure to be used, after which statistical averaging gives the final result.

To summarize, the method of high-resolution prediction of acoustic impedance and lithological estimates below bottom-of-hole is developed using seismic data on

vertical profiles. Frequency band broadening is achieved by stacking the data received from shots with different dominant frequencies. The solution of inverse dynamic problem includes multiples. The impulse seismogram is computed to real scale.

References

ALEKSEYEV, A.S. 1967, Inverse dynamic seismic problems, *in*: Certain Techniques and Algorithms of Interpretation of Geophysical Data, Nauka, Moscow.

BARANOV, V. and KUNETZ, G. 1960, Film synthetic avec réflexions multiples, Théorie et calcul pratique, Geophysical Prospecting 8, 315–326.

GOGONENKOV, G.N., ZAKHAROV, E.T. and ELMANOVICH, S.S. 1980, Prediction of a comprehensive velocity section by seismic data, Applied Geophysics 97, Nedra, Moscow.

LINDSETH, R.O. 1976, Seislog process uses seismic reflection traces, Oil and Gas Journal, Oct. 25, 67–71.

NAHAMKIN, S.A. 1967, On a new method of separation of regular waves in seismic prospecting, Applied Geophysics 50, Nedra, Moscow.

RAINON, E. 1978, Seismic processing VELOG for stratigraphic interpretation. CGG Technical Series, No. 506.78.03.

ROBINSON, E.A. and TREITEL, S. 1967, Principles of digital Wiener filtering, Geophysical Prospecting 15, 311–333.